Cancer Cell
Article

A Mouse Model of Rhabdomyosarcoma Originating from the Adipocyte Lineage

Mark E. Hatley,[1,2,5] Wei Tang,[3] Matthew R. Garcia,[1,2,5] David Finkelstein,[6] Douglas P. Millay,[1] Ning Liu,[1] Jonathan Graff,[3] Rene L. Galindo,[1,2,4,*] and Eric N. Olson[1,*]
[1]Department of Molecular Biology
[2]Department of Pediatrics
[3]Department of Developmental Biology
[4]Department of Pathology
University of Texas Southwestern Medical Center, 5323 Harry Hines Boulevard, Dallas, TX 75390, USA
[5]Department of Oncology
[6]Department of Biostatistics
St. Jude Children's Research Hospital, 262 Danny Thomas Place, Memphis, TN 38105, USA
*Correspondence: rene.galindo@utsouthwestern.edu (R.L.G.), eric.olson@utsouthwestern.edu (E.N.O.)
http://dx.doi.org/10.1016/j.ccr.2012.09.004

SUMMARY

Rhabdomyosarcoma (RMS) is an aggressive skeletal muscle-lineage tumor composed of malignant myoblasts that fail to exit the cell cycle and are blocked from fusing into syncytial muscle. Rhabdomyosarcoma includes two histolopathologic subtypes: alveolar rhabdomyosarcoma, driven by the fusion protein PAX3-FOXO1 or PAX7-FOXO1, and embryonal rhabdomyosarcoma (ERMS), which is genetically heterogeneous. Here, we show that adipocyte-restricted activation of Sonic hedgehog signaling through expression of a constitutively active *Smoothened* allele in mice gives rise to aggressive skeletal muscle tumors that display the histologic and molecular characteristics of human ERMS with high penetrance. Our findings suggest that adipocyte progenitors can be a cell of origin for Sonic hedgehog-driven ERMS, showing that RMS can originate from nonskeletal muscle precursors.

INTRODUCTION

Rhabdomyosarcoma (RMS) is an aggressive skeletal muscle-lineage malignancy and the most common soft tissue sarcoma in children (Barr and Womer, 2009). RMS is comprised of skeletal muscle precursors that fail to exit the cell cycle and are irreversibly blocked from differentiating into syncytial muscle. RMS is typically divided into two histopathologic subgroups, each with distinct clinical features: embryonal RMS (ERMS), which is the more common subtype, and alveolar RMS (ARMS), which is notoriously more aggressive. The genetic lesions that initiate ARMS are well known with three-quarters of ARMS tumors having chromosomal translocations that result in expressing fusion proteins combining the DNA binding domain of either PAX3 or PAX7 transcription factors with the transcriptional activation domain of FOXO1A (Barr, 2001). Because PAX3 and PAX7 have critical roles in normal muscle development, the fusion proteins presumably use the DNA binding domains of the PAX proteins to drive malignant myogensis-related developmental programs (Galindo et al., 2006; Keller and Capecchi, 2005; Wang et al., 2008). ERMS accounts for 75% of RMS cases and is associated with younger age of onset (typically under ten years) and demonstrates a predilection for tissues of the head and neck. The molecular underpinnings and cellular origins of ERMS remain poorly understood. Although most cases of ERMS occur as sporadic, nonheritable tumors, ERMS also associates with familial syndromes caused by mutations in prominent oncogenesis-related signaling pathways, such as p53, Ras, and Sonic hedgehog (Shh) (Estep et al., 2006; Johnson et al., 1996; Li and Fraumeni, 1969).

Significance

Rhabdomyosarcoma is the most common soft tissue malignancy in children. Despite aggressive chemotherapy, radiotherapy, and surgery, clinical outcomes for RMS have not improved for three decades, emphasizing the need to uncover the molecular underpinnings of the disease. Here, we describe a Sonic hedgehog-driven mouse model of ERMS that mimics the histopathological and molecular characteristics of human ERMS, and with notably decreased latency, high penetrance, and a restricted anatomic location when compared to previous models. In addition to yielding mechanistic insights into ERMS, this mouse model also now provides a robust preclinical platform to explore therapeutic strategies to improve RMS treatment.

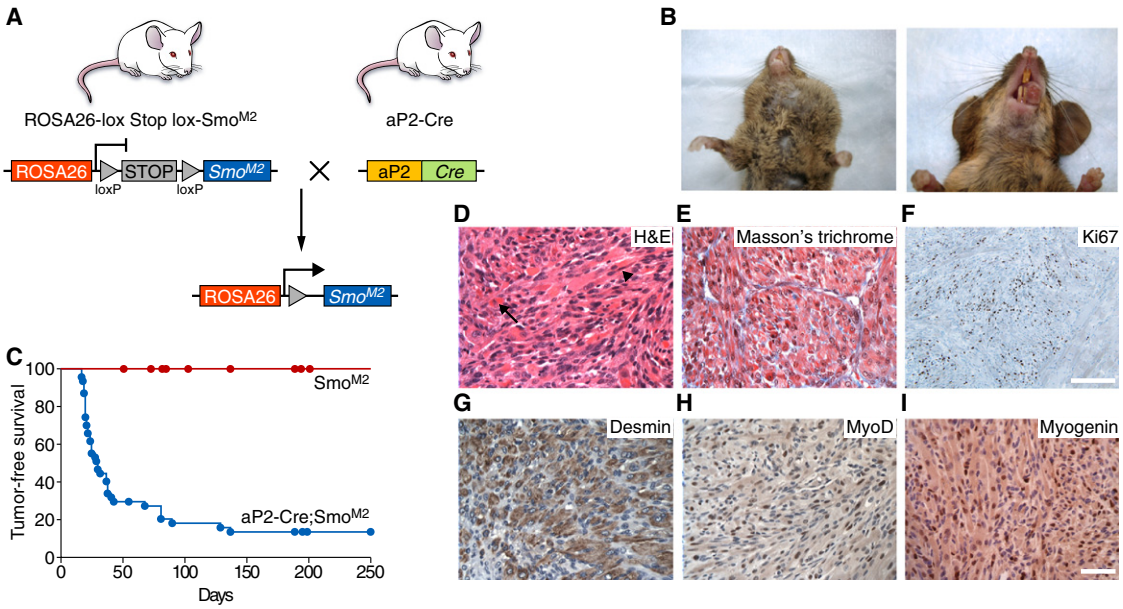

Figure 1. ERMS Caused by Activation of the Sonic Hedgehog Pathway in the aP2 Lineage

(A) Schematic of the conditional *Smo^{M2}* allele and *aP2-Cre*-mediated recombination.

(B) Gross view of tumors in *aP2-Cre;Smo^{M2}* mice.

(C) Kaplan-Meier survival curves illustrated tumor-free survival of *aP2-Cre;Smo$^{M2/+}$* mice (blue line, n = 47) compared to *Smo$^{M2/+}$* littermate controls (red line, n = 19) (p = < 0.0001).

(D) Cross-sectional histology of tumors with H&E staining. Arrow points to rhabdomyoblast and arrowhead points to strap cell.

(E) Masson's trichrome.

(F–I) Sections of tumors immunostained with Ki67, a marker of proliferating cells (F), and Desmin (G), MyoD1 (H), and Myogenin (I), diagnostic of ERMS. Scale bar, 50 μm (D, E, and G–I) and 200 μm (F).

See also Figure S1.

The Shh pathway is an evolutionarily conserved signaling pathway with noted roles in development and in tumorigenesis. Normally, in the absence of extracellular Shh ligand, the Shh signaling pathway is inhibited by the Patched (Ptch) transmembrane receptor, which dominantly represses the Smoothened (Smo) G protein coupled receptor. Upon binding of Shh to Ptch, Smo is freed from Ptch-mediated inhibition and activates the Gli family of transcription factors (Gli1, Gli2, and Gli3) that then drive patterns of gene expression critical for various aspects of development (Lum and Beachy, 2004). Shh-associated diseases include nevoid basal cell carcinoma syndrome (Gorlin syndrome), an autosomal dominant condition caused by heterozygous germ-line mutations in *PTCH1*, which drives basal cell carcinoma, medulloblastoma, and ERMS. Activation of the Shh pathway is also found in spontaneous ERMS tumors, associating with either loss of Shh pathway negative regulators, such as *PTCH1* or *PTCH2* or *Suppressor of Fused* (*SUFU*), or by the activation of the downstream transcriptional effector of Shh signaling, *Gli* (Paulson et al., 2011; Tostar et al., 2006).

Consistent with human ERMS, introducing Shh-pathway-activating mutations in mouse models induces tumorigenesis. Transgenic mice with heterozygous deletion of *Ptch1* develop tumors histologically consistent with ERMS but with a low level of penetrance (10%) (Corcoran and Scott, 2001; Hahn et al., 2000). Mice with heterozygous loss of *Sufu* in combination with *p53* loss develop ERMS with 9% penetrance (Lee et al., 2007). The most robust mouse model of ERMS utilizes a conditional, constitutively activate *Smo* allele (*Smo^{M2}*) controlled by a ubiquitously expressed, inducible Cre transgene, *CAGGS-CreER* (Mao et al., 2006). Although these models point to the involvement of the Shh pathway in the pathogenesis of ERMS, the varied anatomic location, relatively low penetrance of tumorigenesis and occurrence of other tumor types in these models limit their usefulness as a preclinical platform. We have generated a transgenic mouse model in which overexpression of the oncogenic *Smo^{M2}* allele in the adipocyte-restricted aP2 lineage induces tumors that closely resemble human ERMS.

RESULTS

Smo^{M2} Expression in the aP2 Lineage Causes ERMS

We initially sought to explore the role of Shh signaling in adipocyte development and metabolism, using an adipose protein 2 (aP2)-Cre transgenic driver (Tang et al., 2008) to conditionally express constitutively activated Smoothened, Smo^{M2} (Mao et al., 2006) in an adipocytic-specific pattern (Figure 1A). Surprisingly, 80% of mice with the genotype *aP2-Cre;Smo$^{M2/+}$* developed large, aggressive tumors in the head and ventral neck by 2 months of age (Figures 1B and 1C). The tumors ranged in greatest diameter from 1 to 2 cm, were tan/pink/white and solid upon sectioning, and well demarcated from the surrounding nonneoplastic tissue. Histologic examination revealed ERMS-type morphology: the tumors displayed dense cellularity, comprised of a spectrum of cells that were small and round

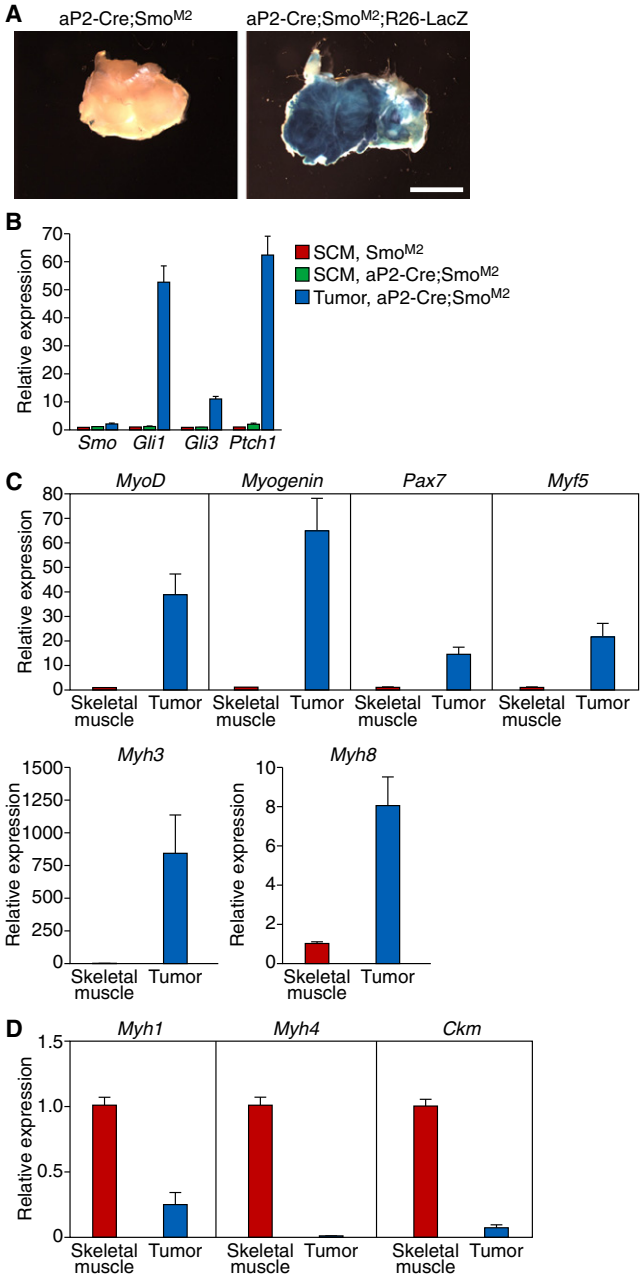

Figure 2. Sonic Hedgehog Activation in *aP2-Cre;Smo^{M2}* Tumors

(A) β-galactosidase enzymatic staining of cross sections of *aP2-Cre;Smo^{M2};R26-LacZ* reporter mouse tumors and *aP2-Cre;Smo^{M2}* tumors illustrating broad homogeneous staining. Scale bar, 5 mm.

(B) Increased expression on Sonic hedgehog pathway target genes in the *aP2-Cre;Smo$^{M2/+}$* tumors compared to mature SCM of *aP2-Cre;Smo$^{M2/+}$* and *Smo$^{M2/+}$* animals by real-time PCR. Data are shown as fold change of gene expression normalized to 18S and expressed relative to SCM of Smo$^{M2/+}$. Results are mean ± SEM (n = 4). p values by two-tailed, unpaired Student's t test are as follows: *Smo* (p = 0.0015), *Gli1* (p < 0.0001), *Gli3* (p < 0.0001), and *Ptch1* (p < 0.0001).

(C and D) Expression of embryonic muscle development genes (C) and markers of terminally differentiated skeletal muscle (D) in *aP2-Cre;Smo$^{M2/+}$* tumors compared to mature SCM as detected by real-time PCR. Data are shown as fold change of gene expression normalized to 18S and expressed relative to SCM of Smo$^{M2/+}$. Results are mean ± SEM (n = 3). p values by two-tailed, unpaired Student's t test are as follows: *MyoD1* (p = 0.0011), *Myogenin* (p = 0.0007), *Pax7* (p = 0.0009), *Myf5* (p = 0.0039), *Myh3* (p = 0.0165), *Myh8* (p = 0.0007), *Myh1* (p < 0.0001), *Myh4* (p < 0.0001), and *Ckm* (p < 0.0001).

to cells that were elongated and spindled, with brightly eosinophilic cytoplasm, pleomorphic nuclei, and visible cross-striations (Figures 1D and 1E). Immunohistochemistry (IHC) for Ki67 showed that the tumor cells were briskly mitotic (Figure 1F). IHC also revealed strong expression of the muscle-specific intermediate filament Desmin and nuclear staining for the muscle-specific transcription factors Myogenin and MyoD1 (Figures 1G–1I). These findings are diagnostic for RMS.

Extensive analyses of the *aP2* promoter in transgenic mice have documented its specificity for the adipocyte lineage and its exclusion from the skeletal muscle lineage (He et al., 2003; Ross et al., 1990; Tang et al., 2008; Urs et al., 2006). Thus, it was surprising to observe RMS tumorigenesis in *aP2-Cre;Smo^{M2}* mice. To test whether *aP2-Cre* activation of the *Smo^{M2}* allele altered or interfered with normal skeletal muscle and/or adipose development, we performed histologic analysis of the sternocleidomastoid (SCM), quadriceps femoris, intrascapular brown fat, and inguinal white fat from 4- to 8-week-old *aP2-Cre;Smo$^{M2/+}$* and *Smo$^{M2/+}$* control mice. We observed no gross abnormalities in muscle or adipose tissue in either cohort (Figure S1 available online). Therefore, activation of the hedgehog pathway by *aP2-Cre*-mediated expression of the *Smo^{M2}* allele did not evoke general defects in myogenesis or adipogenesis.

Activation of Hedgehog Signaling in *aP2-Cre;Smo$^{M2/+}$* Tumors

We analyzed in vivo the expression of the Cre-responsive *R26-LacZ* reporter to confirm that the RMS tumors originate from cell-autonomous activation of the *Smo^{M2}* allele. Intense, homogenous β-galactosidase staining of the tumors revealed that they formed as a consequence of cell-autonomous activation by *aP2-Cre* (Figure 2A). Next, to confirm that the Shh pathway was activated in tumors of *aP2-Cre;Smo$^{M2/+}$* mice, we compared the expression of Shh target genes in control muscle and tumor tissue from both *aP2-Cre;Smo$^{M2/+}$* and *Smo$^{M2/+}$* littermates. The tumors exhibited increased expression of Smo and Shh responsive genes, including *Gli1*, *Gli3*, and *Ptch1* (Figure 2B), whereas gene expression in SCM muscle was unchanged. These findings indicate that the Shh pathway is robustly activated in the ERMS tumors but not in the nonneoplastic skeletal muscle of the *aP2-Cre;Smo$^{M2/+}$* mice, suggesting an origin of tumorigenesis distinct from skeletal muscle lineage precursors.

aP2-Cre;Smo$^{M2/+}$ Tumors Display an Embryonal Muscle Gene Signature

To further determine the extent to which the *aP2-Cre;Smo$^{M2/+}$* tumors resembled ERMS, we isolated RNA from tumor tissue and compared the gene expression profile to that of SCM skeletal muscle of *Smo$^{M2/+}$* littermates. Skeletal muscle regulatory genes (*MyoD1*, *Myogenin*, *Pax7*, and *Myf5)* and embryonic/perinatal myosins (*Myh3* and *Myh8*) displayed markedly increased expression in the *aP2-Cre;Smo$^{M2/+}$* tumors when

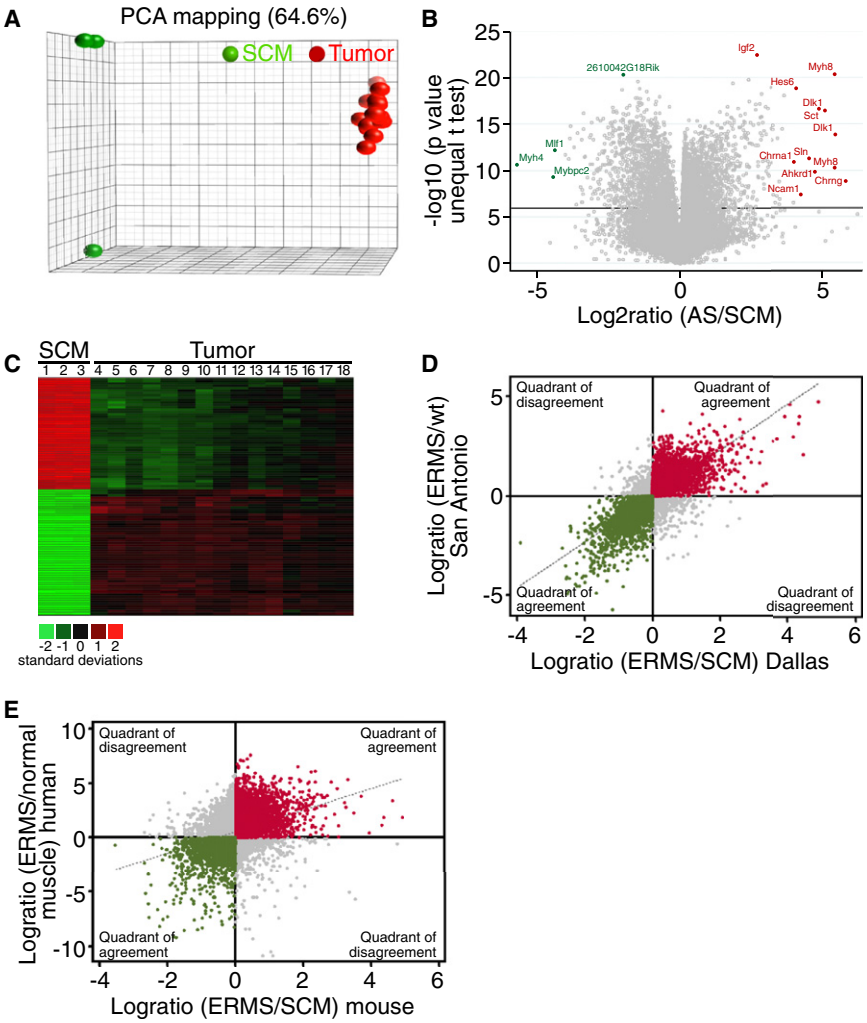

Figure 3. Comparative Transcriptome Analysis of Mouse ERMS and Skeletal Muscle

(A) Principle component analysis (PCA). Three PCA coordinates describe 64.6% of the total data variation (PC1, 52.9%; PC2, 5.99%; and PC3, 5.71%). Red, *aP2-Cre;Smo*$^{M2/+}$ tumors (n = 12). Green, *Smo*$^{M2/+}$ SCM (n = 3).

(B) Volcano plot of the Log_{10} of the p value versus the Log_2 of the fold-difference in expression in the *aP2-Cre;Smo*$^{M2/+}$ tumors compared to the normal skeletal muscle.

(C) Unsupervised hierarchical clustering analysis. Each column represents a distinct sample, and each row represents a distinct gene.

(D) Comparison of *aP2-Cre;Smo*^{M2} tumors to published mouse ERMS models. Gene expressed in both the published mouse ERMS models and the *aP2-Cre;Smo*$^{M2/+}$ tumors (19,878 genes) plotted on graph. Sixty-seven percent of gene pairs show agreement in genes upregulated (red) or downregulated (green) between the previously published mouse ERMS models and the *aP2-Cre;SmoM2* tumors. Spearman correlation = 0.59 and AGDEX = 0.71.

(E) Comparision of *aP2-Cre;Smo*$^{M2/+}$ tumors to human ERMS. Genes expressed in both the published human ERMS and the *aP2-Cre;Smo*$^{M2/+}$ tumors (13,282 genes) plotted on graph. Fifty-eight percent of orthologous gene pairs show agreement in genes upregulated (red) or downregulated (green) between the human ERMS and the *aP2-Cre;SmoM2* tumors. Spearman correlation = 0.29 and AGDEX = 0.3.

See also Figure S2.

compared to the SCM (Figure 2C). In contrast, markers of mature, differentiated skeletal muscle (*Myh1*, *Myh4*, and *Ckm*) were dramatically diminished in *aP2-Cre;Smo*$^{M2/+}$ tumors when compared to SCM (Figure 2D). This embryonal muscle gene expression pattern is consistent with mouse and human ERMS and is indicative of an arrested skeletal myoblastic tissue.

Gene Expression Profiling of *aP2-Cre;Smo*^{M2} Tumors

To further characterize the tumors of the *aP2-Cre;Smo*$^{M2/+}$ mice, we used mRNA expression profiling to compare the gene expression profiles of *aP2-Cre;Smo*$^{M2/+}$ tumors and SCM. The transcriptome of the *aP2-Cre;Smo*$^{M2/+}$ tumors was distinct from that of SCM using principle component analysis to group samples based on gene expression (Figure 3A). Focusing on changes of gene expression with a log_2 ratio greater than 2.5 and a p value less that 0.0001 by Bonferroni, we identified 100 genes that were differentially expressed between *aP2-Cre;Smo*$^{M2/+}$ tumors and normal SCM of *Smo*$^{M2/+}$ littermates (Figures 3B and 3C). Consistent with the developing muscle gene pattern, we noted that perinatal myosin heavy chain *Myh8* was among the genes expressed at high levels in the tumors compared to normal SCM and mature myosin heavy chain *Myh4* was among the genes that exhibited low expression in the tumors compared to SCM (Figures 2 and 3B). These analyses also identified several other genes previously shown to play a role in RMS pathogenesis, including *Igf2*, *Dlk1*, *Ankrd1*, *Chrng*, and *Ncam1* (El-Badry et al., 1990; Gattenloehner et al., 1998; Glüer et al., 1998; Ishiguro et al., 2008; Rezvani et al., 2012). Real-time PCR validation of the array is shown in Figure S2A.

During muscle development, a subset of myogenic progenitors forgoes terminal differentiation and instead become mononuclear satellite cells associated with the myofiber basal lamina. Muscle satellite cells are responsible for the postnatal growth, repair, and maintenance of skeletal muscle (Seale and Rudnicki, 2000). Satellite cells remain quiescent until activated by muscle injury, when they serve as muscle-specific stem cells that generate myogenic precursors and repair injured muscle (Shadrach and Wagers, 2011). Mice with loss-of-function of *p53* and gain-of-function of the Shh pathway through the loss of *Ptch1* in myoblasts and satellite cell lineages develop tumors that resemble human ERMS and display a gene expression signature consistent with satellite cell activation (Rubin et al., 2011). Interestingly, the tumors arising from the adipocyte-specific *aP2-Cre* driver expressed numerous genes associated with satellite cell activation (Fukada et al., 2007), including *Rho GDP dissociation inhibitor gamma* (*Arhgdig*), *ankyrin repeat*

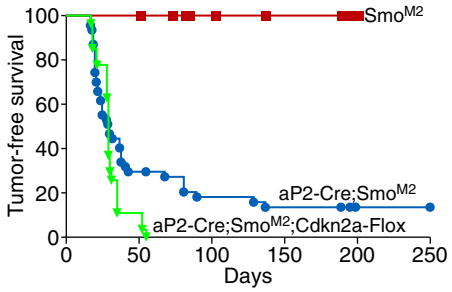

Figure 4. *Cdkn2a* Loss Cooperates in *aP2-Cre;Smo^{M2}* Mouse Tumors

Kaplan-Meier survival curves illustrate tumor-free survival of *aP2-Cre;Smo$^{M2/+}$;Cdkn2a^{Flox}* mice (green line, n = 27) compared to data from Figure 1C *aP2-Cre;Smo$^{M2/+}$* (blue line, n = 47) and *Smo$^{M2/+}$* littermate controls (red line, n = 19). p = 0.0337.

domain 1 (*Ankrd1*), (*fetal*) *nicotinic cholinergic receptor gamma polypeptide* (*Chrng*), *distal-less homeobox 2* (*Dlx2*), *hairy and enhancer of split* (*Hes6*), *low density lipoprotein receptor-related protein 4* (*Lrp4*), *Otogelin* (*Otog*), *Secretin* (*Sct*), *troponin C* (*Tnnc1*), *troponin T1* (*Tnnt1*), *cardiac troponin T2* (*Tnnt2*), and *unc-5 homolog B* (*Unc5b*) (Figure S2B). Twenty percent of all the genes with increased expression of 5-fold or greater in the *aP2-Cre;Smo$^{M2/+}$* tumors display increased expression in activated satellite cells compared to quiescent satellite cells. Thus, despite arising from the aP2 adipocyte lineage, the *aP2-Cre;Smo$^{M2/+}$* tumors displayed a gene expression profile similar to other murine ERMS models and activated satellite cells. These findings suggest that the satellite cell gene expression signature is likely reflective of the ERMS tumor pathology rather than the cell type of origin of the tumor.

To further test how the *aP2-Cre;Smo$^{M2/+}$* tumors resemble previously reported mouse ERMS models, we compared the gene expression pattern of our model to that of previously published mouse ERMS. The comparison group contained mouse tumors that developed from the conditional deletion of *Ptch1$^{flox/+}$* and *Trp53$^{flox/flox}$* alleles with *Myf5-Cre*, *Pax3-Cre*, and *Pax7-CreERp*, respectively (Rubin et al., 2011). Overall, 67% of the 19,878 probe pairs showed agreement in gene expression between our model and the previously published models (Figure 3D). Next, we used cross-species comparison of the mouse and human ERMS transcriptomes to determine how closely the *aP2-Cre;Smo$^{M2/+}$* tumors resemble human ERMS. We observed a statistically significant match between the mouse *aP2-Cre;Smo$^{M2/+}$* tumors and human ERMS (Figure 3E). Of the 13,282 ortholog gene pairs, 58% showed agreement in gene expression between mouse and human. Together, these data confirm that the *aP2-Cre;Smo$^{M2/+}$* mouse tumors accurately model the transcriptome of both previously published mouse models and human ERMS.

Cooperativity between Smo^{M2} Activation and Cdkn2a Loss

The tumor suppressor *CDKN2A* is one of the most commonly mutated alleles in human cancer (Beroukhim et al., 2010; Bignell et al., 2010). Homozygous deletions of *CDKN2A* have been reported in ERMS (Chen et al., 2007; Iolascon et al., 1996; Paulson et al., 2011; Williamson et al., 2010). To test for potential cooperativity between *Cdkn2a* and hedgehog-driven ERMS, we intercrossed a conditional *Cdkn2a^{Flox}* allele into our model (Aguirre et al., 2003). *aP2-Cre;Cdkn2a$^{Flox/Flox}$* mice did not develop ERMS, whereas deletion of *Cdkn2a* in *aP2-Cre;Smo$^{M2/+}$;Cdkn2a$^{Flox/Flox}$* mice triggered decreased latency and increased penetrance of tumorigenesis with all mice having tumors by 55 days (Figure 4). These results demonstrate that the Shh pathway and Cdkn2a can actively drive ERMS oncogenicity in vivo.

Sonic Hedgehog Activation in the Embryonic Muscle Lineage and Postnatal Satellite Cells

We next crossed the *Smo^{M2}* allele to mice bearing several muscle lineage-restricted Cre-drivers to determine whether activation of the Shh pathway by expression of the Smo^{M2} oncogene in the muscle lineage would phenocopy the tumors of the *aP2-Cre;Smo$^{M2/+}$* mice. Activation of the *Smo^{M2}* allele early in muscle development with *Myf5-Cre*, *Pax3-Cre*, or *MyoD1-Cre* resulted in embryonic lethality without tumor formation, whereas mice with activation of *Smo^{M2}* in terminally differentiated skeletal muscle with *MCK-Cre* were viable with no evidence of tumorigenesis (Figure S3).

In contrast, activation of *Smo^{M2}* with *Myogenin-Cre*, which is specific for early muscle differentiation, resulted in tongue tumors in 100% of the mice (Figure 5A) but no tumors in the anterior neck, as seen in *aP2-Cre;Smo$^{M2/+}$* mice. Specifically, the *Myogenin-Cre;Smo$^{M2/+}$* mice were runted compared to littermates and were sacrificed between 19 and 39 days for lack of weight gain and ill appearance. None of the *Myogenin-Cre;Smo$^{M2/+}$* mice had visible tumors prior to sacrifice; however, all *Myogenin-Cre;Smo$^{M2/+}$* mice had tumors visible upon necropsy throughout the tongue (Figure 5B). The *Myogenin-Cre;Smo$^{M2/+}$* tumors appeared histologically similar to the *aP2-Cre;Smo$^{M2/+}$* tumors and stained positive both MyoD1 and Myogenin. We detected no significant difference in the gene expression profile of the *Myogenin-Cre;Smo$^{M2/+}$* tumors and the *aP2-Cre;Smo$^{M2/+}$* (Figures 5C and 5D). The embryonic lethality of Smo^{M2} expression early in muscle development with *Myf5-Cre*, *Pax3-Cre*, and *MyoD1-Cre* and the more aggressive phenotype with the *Myogenin-Cre* suggests that *aP2-Cre* does not globally activate Smo^{M2} expression in the muscle lineage.

Previous studies illustrate that satellite cells are a potential origin for ERMS (Hettmer et al., 2011; Rubin et al., 2011; Tiffin et al., 2003). Given the activated satellite cell signature of the *aP2-Cre;Smo$^{M2/+}$* tumors, we sought to formally test whether satellite cells are an origin of the *aP2-Cre;Smo$^{M2/+}$* tumors. The *Pax7-CreER^{T2}* allele allows for specific Smo^{M2} postnatal induction in both quiescent and activated satellite cells (Lepper et al., 2009). We crossed the Smo^{M2} mouse with the satellite cell Cre-driver, *Pax7-CreER^{T2}* and administered tamoxifen at day-of-life 1 or day-of-life 14 (Figure S3G). Gene expression from the SCM containing only a small fraction of satellite cells from the *Pax7-CreER^{T2};Smo$^{M2/+}$* and *Smo$^{M2/+}$* Cre-negative littermates revealed that the Smo^{M2} (that has a carboxy terminal YFP fusion) was activated following tamoxifen administration (Figure S3H). None of the *Pax7-CreER^{T2};Smo$^{M2/+}$* animals injected with tamoxifen at either day 1 (n = 8) or day 14 (n = 9)

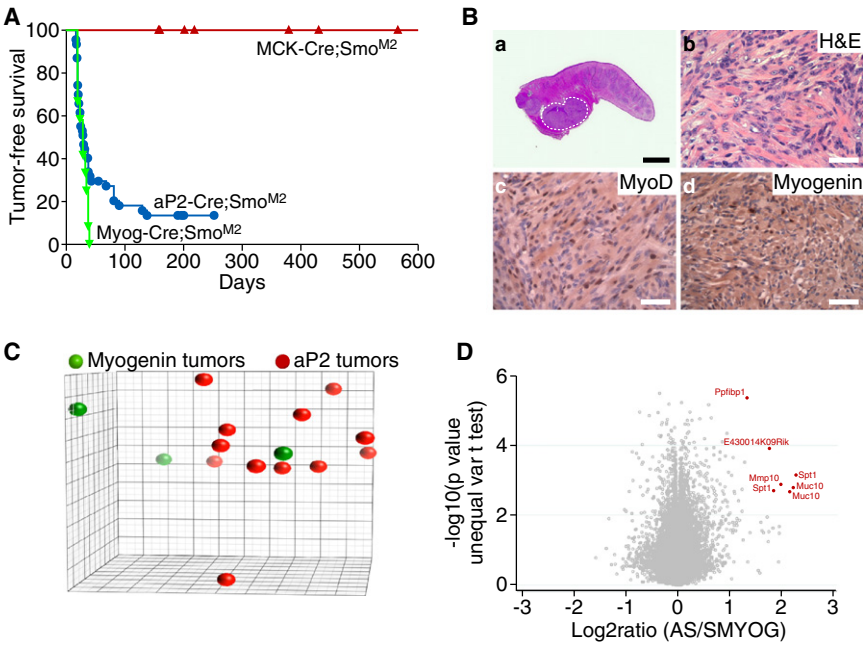

Figure 5. Tongue ERMS in *Myogenin-Cre;Smo^{M2}* Mice

(A) Kaplan-Meier survival curves illustrated tumor-free survival of *Myogenin-Cre;Smo$^{M2/+}$* mice (green line, n = 12) and of *MCK-Cre;Smo$^{M2/+}$* (red line, n = 18) compared to tumor-free survival of *aP2-Cre;Smo$^{M2/+}$* from Figure 1C (blue line).

(B) Tumor histology. (a) Gross cross-section of tongue with tumor outlined by white, dashed line. (b) H&E section illustrating cross striations. (c and d) Immunochemistry illustrating nuclear MyoD1 and Myogenin. Scale bars, 2 mm (a) and 50 μm (b, c, and d).

(C) Principle component analysis for mouse *Myogenin-Cre;Smo$^{M2/+}$* tumors (green, n = 3) and *aP2-Cre;Smo$^{M2/+}$* tumors (red, n = 12).

(D) Volcano plot of the Log_{10} of the p value versus the Log_2 of the fold-difference in expression in the *aP2-Cre;Smo$^{M2/+}$* tumors compared to the *Myogenin-Cre;Smo$^{M2/+}$* tumors.

See also Figure S3.

developed tumors by 150 days, arguing against the satellite cell population as the origin of the ERMS in the *aP2-Cre;Smo$^{M2/+}$* model.

aP2-Cre Is Active in Adipose Tissue but Not Skeletal Muscle

The development of tumors that resemble human ERMS from activation of the oncogenic *Smo^{M2}* allele in the aP2 adipocyte lineage was surprising. However, despite arising from the *aP2* lineage, the *aP2-Cre;Smo$^{M2/+}$* tumors did not express *aP2* or other genes of the adipocyte lineage (Figure S4A). Consistent with previous reports, we determined that *aP2* is expressed in the progenitors from the stromal vascular fraction of brown adipose tissue (BAT) and white adipose tissue (WAT), as well as mature adipocytes. However, *aP2* was not expressed from satellite cells or the SCM, gastrocnemius, or quadriceps femoris skeletal muscles (Figure S4B). The *aP2-Cre* transgenic used in this study was previously characterized and reported not to be expressed in the muscle lineage (Tang et al., 2008). Moreover, the identical 5.4 kb *aP2* promoter element was previously shown to be adipose-specific and to result in hibernoma formation, not ERMS, when fused to simian virus 40 Large T antigen (He et al., 2003; Ross et al., 1990, 1992). Another *aP2-Cre* transgene containing the same 5.4 kb *aP2* promoter has also been shown to be inactive in the muscle lineage but to be active primarily in BAT and WAT and in the developing cartilage, vertebra, and dorsal root ganglia (He et al., 2003; Urs et al., 2006).

To confirm the pattern of expression of *aP2-Cre* and to further define the origins of tumors in the *aP2-Cre;Smo$^{M2/+}$* mice, we again turned to *aP2-Cre;R26-LacZ* reporter mice. The *aP2-Cre* was activated in both BAT and WAT but showed no detectable expression in skeletal muscle (Figure 6A), suggesting that RMS in these mice arises from a nonskeletal muscle origin. We compared the gene expression in isolated intrascapular BAT, inguinal WAT, SCM, and gastrocnemius skeletal muscle, and tumor from the *aP2-Cre;Smo$^{M2/+}$* and *Smo$^{M2/+}$* Cre-negative littermates. Although the oncogenic *Smo^{M2}* allele was activated in the fat lineage, the tumors did not express adipocyte lineage genes, such as *aP2*, *Pparγ*, and *Ucp1* (Figures S4C–S4E). Also, the normal skeletal muscle from the *aP2-Cre;Smo$^{M2/+}$* mice did not display increased Smo and Shh target genes, suggesting that Smo^{M2} was not activated in the muscle lineage.

To further test whether the *aP2-Cre* transgene is inactive in skeletal muscle, we bred *aP2-Cre* mice to an additional reporter allele, *R26-YFP*. A western blot for YFP of whole tissue lysates of isolated intrascapular BAT, inguinal WAT, and SCM from *aP2-Cre;R26-YFP* and *R26-YFP* littermates at P28 demonstrated no evidence of YFP expression in skeletal muscle (Figures S4F and S4G). Together, these data illustrate that the *aP2-Cre* transgene is not expressed in skeletal muscle, consistent with the notion that the *aP2-Cre;Smo$^{M2/+}$* ERMS tumors originate outside the skeletal muscle lineage.

ERMS in Adipose Tissue

To better delineate the tissue compartment giving rise to the *aP2-Cre;Smo^{M2}* ERMS tumors, we sacrificed animals at P14, before tumor masses were grossly visible, with the notion of capturing microscopic foci of RMS arising in situ. The dissected SCM of a representative animal contained a small nodule clearly distinct from adjacent normal brown and white adipose tissues and SCM skeletal muscle (Figure 6B). The developing tumor was completely surrounded by nonneoplastic adipose tissue adjacent to and clearly separated from the SCM. The tumor displays the same appearance and histological characteristics as the previously described *aP2-Cre;Smo$^{M2/+}$* tumors. These findings further support the notion that the ERMS in the *aP2-Cre;Smo$^{M2/+}$* mice develop outside of the muscle lineage.

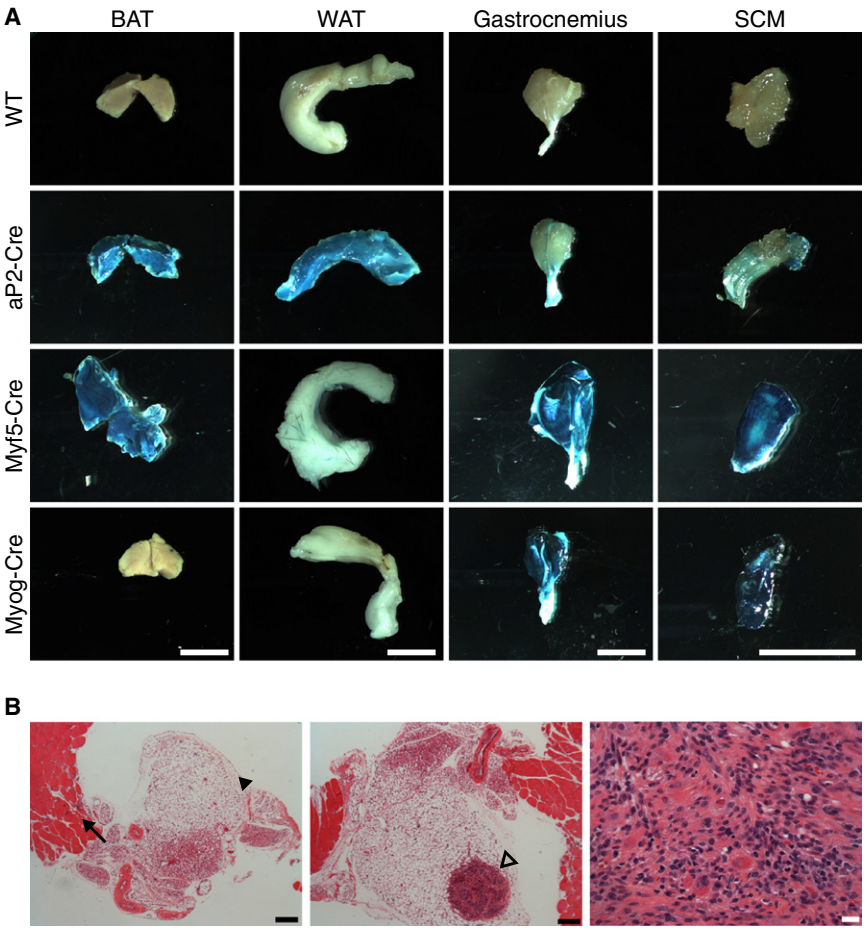

Figure 6. aP2-Cre Expression in Fat Lineages and *aP2-Cre;Smo^{M2}* Tumors in Adipose Tissue Adjacent to Muscle

(A) Mice bearing Cre-drivers *aP2-Cre*, *Myf5-Cre*, and *Myogenin-Cre* were bred to R26-LacZ reporter mice. The BAT, WAT, gastrocnemius, and SCM were isolated from P28 mice and stained with X-gal to determine β-galactosidase activity. Scale bars, 5 mm.

(B) Serial sections through neck tissue with a visible node at P14 on necropsy and stained with H&E. (Left) Level below nodule illustrating normal SCM and adjacent adipose tissue. Arrow and arrowhead point to SCM and adipose tissue, respectively. Scale bar, 200 μm. (Middle) Section illustrating the tumor isolated within the adipose tissue. The open arrowhead points to tumor. Scale bar, 200 μm. (Right) High power view of tumor. Scale bar, 20 μm.

See also Figure S4.

DISCUSSION

Through adipocyte-restricted activation of the hedgehog pathway, we have developed a highly efficient mouse model of ERMS. Our findings demonstrate that constitutive activation of the hedgehog pathway by an oncogenic *Smoothened* allele in the aP2 adipocyte lineage of mice results in the formation of aggressive head and neck tumors that mimic human ERMS histologically and molecularly. Though we cannot completely exclude the unlikely possibility that *aP2-Cre* is expressed in a rare population of myogenic cells, together these findings strongly argue that ERMS driven by the Shh pathway can originate from tissue histologically distinct from muscle.

Although activation of the Shh pathway inhibits fat formation in invertebrates and mammalian cellular models acting upstream of PPARγ (Suh et al., 2006), the Shh pathway has well documented roles in skeletal muscle development and in the pathogenesis of ERMS (Barlow et al., 1997; Fan and Tessier-Lavigne, 1994; Johnson et al., 1994; Münsterberg et al., 1995; Zibat et al., 2010). The role of the Shh pathway in the development of ERMS is also supported by human cancer predisposition syndromes that result in Shh pathway activation and recent genomic interrogation of human ERMS samples. Gorlin syndrome, or nevoid basal cell carcinoma syndrome, is a human genetic disorder resulting from germline inactivating mutations of *PTCH1*, which encodes a negative regulator of the Shh pathway and displays an increased incidence of ERMS. Increased expression of *GLI1* and *PTCH1* in ERMS compared to ARMS has been reported (Paulson et al., 2011; Pressey et al., 2011). Zibat et al. (2010) found that high levels of expression of Shh target genes, *PTCH1*, *GLI1*, *GLI3*, and *MYF5* are a common feature of ERMS and fusion gene-negative ARMS and not of fusion gene-positive ARMS. High expression of *PTCH1* also correlated with poor survival (Zibat et al., 2010). These findings illustrate that the hedgehog pathway influences RMS pathogenesis.

The tumor-free survival curve of the *aP2-Cre;Smo$^{M2/+}$* mice displays a biphasic appearance with some mice never developing tumors. The early development of tumors with approximately 50% of mice exhibiting tumors by 28 days of life shows that activation of *Smo^{M2}* is sufficient to initiate ERMS tumorigenesis. However, the incomplete penetrance of the model suggests that other genetic "hits" are likely necessary for complete neoplastic transformation and/or tumor progression. For example, the tumor suppressor *CDKN2A* encoding p16^{INK4A} and p14^{ARF} (p19^{Arf} in mice) is commonly deleted in human ERMS, which causes concomitant deregulation of the Rb and p53 pathways (Chen et al., 2007; Iolascon et al., 1996; Paulson et al., 2011). Deletion of *Cdkn2a* was previously shown to cooperate with a c-Met-driven ERMS mouse model (Sharp et al., 2002). The deletion of *Cdkn2a* in the *aP2-Cre;Smo$^{M2/+}$* model resulted in complete penetrance, illustrating cooperativity between the Shh pathway and Ink4a/Arf in RMS.

Through mouse crosses deleting *Ptch1* and *p53* with multiple muscle-specific Cre drivers, Rubin et al. (2011) recently demonstrated that ERMS developed upon inactivating these loci in muscle stem cells (satellite cells), as well as proliferating and maturing myoblasts. All ERMS tumors exhibited the same gene

signature despite the cell of origin of the tumors, suggesting that the gene expression profile was more reflective of the final state of the tumor rather than the lineage from which it arose (Rubin et al., 2011). Though the *aP2-Cre* transgene is not active in the muscle lineage, the gene expression profile of the ERMS from *aP2-Cre;Smo*$^{M2/+}$ mice is remarkably similar to previous murine ERMS models and to that of human ERMS. Thus, in multiple and seemingly unrelated settings, activated satellite gene signatures are seen in both mouse and human ERMS.

To address whether satellite cells were the origin of the *aP2-Cre;Smo*$^{M2/+}$ tumors, we utilized the *Pax7-CreER*^{T2} allele. Pax7 along with Pax3 play a critical role in the developing skeletal muscle, where both Pax7- and Pax3-positive cells in the dermomyotome give rise to the embryonic and fetal myoblasts that form the primary and secondary muscle fibers. Consistent with these observations, we show that using *Pax3-Cre* to activate the *Smo*^{M2} allele during development causes embryonic lethality. Also, using Cre-drivers (*Myf5-Cre* and *MyoD1-Cre*) that act downstream of Pax7 during myogenesis also caused embryonic lethality. Thus, in lieu of using the *Pax7-CreER*^{T2} allele to induce Smo^{M2} expression embryonically, which would globally disrupt muscle patterning and cause potent embryonic lethality, we focused on tamoxifen-induced activation of the *Pax7-CreER*^{T2}*;Smo*$^{M2/+}$ alleles in newly born pups, a time point at which Pax7 becomes restricted to the satellite cell lineage. Indeed, lethality was circumvented by this approach, which allowed for viable animals to be profiled for tumorigenesis. This dedicated restricted activation of the oncogenic Smo^{M2} allele in the Pax7^{+} satellite cells did not result in tumor formation. If *aP2-Cre* was expressed at a level that was completely undetectable in either of the lineage tracing experiments with the R26-LacZ or R26-YFP mice in the satellite cells, and the satellite cells were the origin of these tumors, one would expect that oncogene activation in the satellite cell lineage would phenocopy the *aP2-Cre;Smo*$^{M2/+}$ tumors, which was not observed.

The cell of origin of ERMS has been and continues to be ambiguous (Hettmer and Wagers, 2010). It is generally thought that ERMS develops from cells of the muscle lineage, given that ERMS express skeletal muscle markers, such as MyoD, Myogenin, and Desmin. However, an origin restricted to muscle progenitors does not explain how ERMS occurs in locations that lack striated muscle, such as the prostate, urinary bladder, and the biliary tree (Heyn et al., 1997; Spunt et al., 2000). Transdifferentiation of mesenchymal progenitor cells, including progenitors of the adipose lineage into ERMS, could account for ERMS that arise in tissues that normally lack skeletal muscle, such as the biliary and genitourinary tract. Transdifferentiation of lineages not fated to become skeletal muscle could also explain the appearance of arrested skeletal muscle development, as lineages that transdifferentiate after their fate has been initially established could lack the developmental priming necessary to terminally differentiate into striated skeletal muscle.

Recent reports suggest that skeletal muscle and brown fat share a developmental ancestry (Atit et al., 2006; Kajimura et al., 2009; Seale et al., 2008). In humans, brown fat has traditionally been thought to be restricted to newborns. However, recent reports have shown that brown adipose tissue, located primarily in the supraclavicular neck, is readily activated upon cold exposure in adult humans (Cypess et al., 2009; van Marken Lichtenbelt et al., 2009; Virtanen et al., 2009). We speculate that constitutive activation of the Shh pathway by Smo^{M2} derails brown adipocyte progenitors into the muscle lineage, such that the resulting cells lack the previous developmental priming and necessary modifications to develop normally into mature skeletal muscle and thus display an arrested state of skeletal muscle development or ERMS.

The rhabdomyosarcoma tumors in *aP2-Cre;Smo*$^{M2/+}$ mutant mice closely resemble human rhabdomyosarcoma with respect to location, histology, and gene expression. We postulate that the relatively short latency and high penetrance of ERMS in this model now provides an efficient genetic system and tool for the analysis of RMS modifiers and provides a unique platform for preclinical studies.

EXPERIMENTAL PROCEDURES

Mouse Strains

All mice used in this study have been previously reported: *aP2-Cre* (Tang et al., 2008), *Smo*^{M2} (Jackson Laboratories, Bar Harbor, ME, USA; #5130) (Mao et al., 2006), *Cdkn2a*^{Flox} (Aguirre et al., 2003), *Pax3-Cre* (Jackson Laboratories, #5549) (Engleka et al., 2005), *Myf5-Cre* (Jackson Laboratories, #7893) (Tallquist et al., 2000), *MyoD1-Cre* (Jackson Laboratories, #14140) (Yamamoto et al., 2009), *Myogenin-Cre* (Li et al., 2005), *MCK-Cre* (Jackson Laboratories, #6475) (Brüning et al., 1998), *Pax7-Cre*^{ERT2} (Jackson Laboratories, #12476) (Lepper et al., 2009) *R26-LacZ* (Jackson Laboratories, #3474) (Soriano, 1999), and *R26-YFP* (Jackson Laboratories, #6148) (Srinivas et al., 2001). *aP2-Cre;Smo*$^{M2/+}$ mice were generated by breeding *aP2-Cre* male animals to *Smo*$^{M2/M2}$ females. *aP2-Cre;Smo*$^{M2/+}$*;Cdkn2a*$^{Fl/Fl}$ mice were generated by breeding *aP2-Cre;Cdkn2a*$^{Fl/Fl}$ males with *Smo*$^{M2/M2}$*;Cdkn2a*$^{Fl/Fl}$ females. All mice used in these studies were of mixed genetic backgrounds, and all comparisons were performed on littermate controls. The end point for the Kaplan-Meier tumor-free survival analysis was the first visible sign of tumor. All experimental procedures involving animals in this study were reviewed and approved by the Institutional Animal Care and Research Advisory Committee at the University of Texas Southwestern Medical Center.

Histology and Immunohistochemistry

Dissected tumors were fixed in 10% neutral-buffered formalin, placed in fixative overnight, embedded in paraffin, and sectioned at 5 μm intervals. Hematoxylin and eosin (H&E) and Trichrome stains were performed using standard procedures. All paraffin-embedded sections for immunohistochemistry were deparaffinized, heated in a microwave in 0.01 M sodium citrate buffer for antigen retrieval, treated with 3% H_2O_2 for 10 min, and rinsed in H_2O and PBS. For Ki-67 immunohistochemistry, sections were blocked in 5% goat serum in PBS, followed by incubation with anti-Ki67 antibody (Abcam, Cambridge, UK; ab15580) at a concentration of 1:100. Signals were detected with a Vectastain ABC kit (Vector Laboratories, Burlingame, CA, USA) and 3,3′-diaminobenzidine (DAB) substrate (Vector Laboratories). Sections were counterstained with hematoxylin and mounted. For MyoD, Myogenin, and Desmin immunohistochemistry, the M.O.M. Immunodetection Kit (Vector Laboratories), Vectastain Elite kit (Vector Laboratories), and 3,3′-diaminobenzidine (DAB) substrate were used. The MyoD1 primary antibody (Dako, Carpinteria, CA, USA; 5.8A, M3512) was used at a concentration of 1:50, the Myogenin primary antibody (Dako, 5FD, M3559) was used at a concentration of 1:25, and the Desmin primary antibody (Developmental Hybridoma Bank, D3 supernatants) was used at a concentration of 1:100.

LacZ Staining

β-galactosidase expression was detected in isolated tissue fixed for 1 hr in 4% paraformaldehyde, 0.1 M phosphate buffer (pH 7.4), 0.01% sodium deoxycholate, and 0.02% Nonidet P-40 and then washed twice with buffer (0.1 M phosphate buffer [pH 7.4], 0.01% sodium deoxycholate, and 0.02% Nonidet P-40). β-galactosidase was detected by overnight incubation at

room temperature in 1 mg/ml X-gal (5-bromo-4-chloro-3-indoyl-β-D-galactoside), 5 mM potassium ferricyanide, and 5 mM potassium ferrocyanide, 2 mM $MgCl_2$, 0.01% sodium deoxycholate, and 0.02% Nonidet P-40. Tissues were rinsed twice in buffer and postfixed overnight in 4% paraformaldehyde and 0.2% glutaraldehyde.

RNA Purification, RT-PCR, and Real-Time PCR

Total RNA was isolated from normal SCM or tumors with Trizol reagent (Invitrogen, Carlsbad, CA, USA) in accordance with the manufacturer's protocol. Reverse transcription was performed using random hexamer primers and SuperScript III First-Strand Synthesis (Invitrogen). Real-time PCR was performed using SYBR Green assay on an ABI-PE Prism 7900HT sequence detection system in accordance with manufacturer's protocol. The relative quantities of the gene of interest were determined using the $\Delta\Delta C_T$ method and were normalized to 18S and expressed relative to the value for the normal SCM or to brown adipose tissue. In all real-time PCR assays, each group contained four independent samples assayed in duplicate.

Microarray Analysis

RNA from *aP2-Cre;Smo*$^{M2/+}$ tumors or SCM with quality verified with nanodrop and bioanalyzer was hybridized to the Illumina MouseWG-6 v2.0 BeadChip. Normalized signal data from Illumina Whole-Genome Gene Expression BeadChips were collated and log base 2 transformed in STATA/SE 11.2 (College Station, TX, USA). Next, the data was imported into Partek Genomic Suite 6.6 (St. Louis, MO, USA) visualized by principal components analysis (PCA) to check for consistency of samples and class variance. The log2 transformed *aP2-Cre;Smo*$^{M2/+}$ tumor and SCM data were batch corrected and then compared. Using Partek, each probeset was compared by an unequal variance t test. The Bonferroni correction was then applied. This same process was repeated for *aP2-Cre;Smo*$^{M2/+}$ and *Myogenin-Cre;Smo*$^{M2/+}$ data.

Probesets that passed the Bonferroni cutoff at 0.0001 in the *aP2-Cre;Smo*$^{M2/+}$ tumor, SCM comparison, and had an absolute value of the log2ratio >2.5 were selected for the heat map. Using Spotfire Decision Site 9.1.2, the data were z transformed and hierarchically clustered using Euclidean distance; data was then recolored to the fixed −2 to 2 scale. The volcano plot was produced in STATA/SE 11.2 by first −log10 transforming the p value from the unequal variance t test. The transformed score was then plotted against the log2ratio of expression from the two classes. The horizontal line represents the 0.05 Bonferroni cutoff, and the colors represent select significantly differential genes that are either elevated (red) in *aP2-Cre;Smo*$^{M2/+}$ tumor relative to SCM or downregulated (green). The volcano plot for the *aP2-Cre;Smo*$^{M2/+}$*/Myogenini-Cre;Smo*$^{M2/+}$ t test results was created in the same manner. Although in this case, no genes had statistically significant differences. Gene expression was confirmed by real-time PCR.

Cross-Species and Mouse Model Expression Comparisons

The human data comes from two distinct studies: the 36 ERMS samples from the Curie Institute (Williamson et al., 2010) and Vastus Lateralis muscle of ten young trained subjects from the Mayo clinic (GSE9103). Both human studies used the Affymetrix Human Genome U133 Plus 2.0 Arrays. Data was rma summarized for each group independently (Partek Genomics Suite 6.6). Next, ERMS/wt-muscle log ratios were calculated and median normalized to center at zero to correct for source effects. The 15 mouse tumors and 3 normal SCM samples from this study were assayed by Illumina MouseWG-6 v2.0 BeadChip. Log2ratios were calculated, and the cross-species cross-platform data were matched by unigene ID based on an Affymetrix cross-species unigene file derived from NCBI homologene data. Whenever multiple probes were designated for a given unigene in either species, the probe with the maximum average expression was retained yielding 13,282 logratio pairs. The Spearman Correlation, AGDEX (Johnson et al., 2010), and linear fit were calculated and graphically depicted using STATA/SE 11.

The mouse model comparison was within species, but the cross two version comparison above was used. The San Antonio model was performed on the Illumina mouseRef-8 v1.1 expression beadchip. For the with intraspecies comparison, four normal skeletal muscle samples and seven ERMS samples from San Antonio were compared to our model data. Probe matching was direct by Illumina ID yielding 19,878 pairs. AGDEX, Spearman correlation, and linear fit were calculated and graphed as in the cross-species example.

Statistical Analysis

Results are expressed as the mean ± SEM. We utilized a two-tailed, unpaired Student's t test for all pairwise comparisons (GraphPad Prism version 5). p values less than 0.05 were considered significant.

ACCESSION NUMBERS

Illumina data for the mouse ERMS and SCM can be found in the Gene Expression Omnibus database under number GSE40359.

SUPPLEMENTAL INFORMATION

Supplemental Information includes four figures and Supplemental Experimental Procedures and can be found with this article online at http://dx.doi.org/10.1016/j.ccr.2012.09.004.

ACKNOWLEDGMENTS

We are grateful to Jose Cabrera for figure preparation and John Shelton for experimental assistance. We thank Nabeel Bardeesy for the *Cdkn2a*^{Flox} mice. Work in E.N.O.'s laboratory was supported by grants from the National Institutes of Health, the Leducq Foundation, the Robert A. Welch Foundation, and the Cancer Prevention and Research Institute of Texas. M.E.H. is supported by Alex's Lemonade Stand Foundation, Pediatric Scientist Development Program sponsored by the *Eunice Kennedy Shriver* National Institute of Child Health and Human Development (NICHD Grant Award K12-HD000850), and the American Lebanese Syrian Associated Charities (ALSAC). Funding to R.L.G. for this work was provided by the Burroughs Wellcome Fund Career Award for Medical Scientists, the American Cancer Society/Simmons Cancer Center Institutional Research Grant (ACS-IRG-02-196), The CureSearch for Children's Cancer Young Investigator Program, and an Alex's Lemonade Stand Foundation "A" Award. Work in J. G.'s lab was supported by NIDDK Grants R01-DK066566, R01-DK064261, and R01-DK088220.

Received: April 20, 2012
Revised: July 17, 2012
Accepted: September 4, 2012
Published: October 15, 2012

REFERENCES

Aguirre, A.J., Bardeesy, N., Sinha, M., Lopez, L., Tuveson, D.A., Horner, J., Redston, M.S., and DePinho, R.A. (2003). Activated Kras and Ink4a/Arf deficiency cooperate to produce metastatic pancreatic ductal adenocarcinoma. Genes Dev. *17*, 3112–3126.

Atit, R., Sgaier, S.K., Mohamed, O.A., Taketo, M.M., Dufort, D., Joyner, A.L., Niswander, L., and Conlon, R.A. (2006). Beta-catenin activation is necessary and sufficient to specify the dorsal dermal fate in the mouse. Dev. Biol. *296*, 164–176.

Barlow, C., Schroeder, M., Lekstrom-Himes, J., Kylefjord, H., Deng, C.X., Wynshaw-Boris, A., Spiegelman, B.M., and Xanthopoulos, K.G. (1997). Targeted expression of Cre recombinase to adipose tissue of transgenic mice directs adipose-specific excision of loxP-flanked gene segments. Nucleic Acids Res. *25*, 2543–2545.

Barr, F.G. (2001). Gene fusions involving PAX and FOX family members in alveolar rhabdomyosarcoma. Oncogene *20*, 5736–5746.

Barr, F.G., and Womer, R.B. (2009). Rhabdomyosarcoma. In Oncology of Infancy and Childhood, S.H. Orkin, D.E. Fisher, A.T. Look, S.E. Lux, D. Ginsburg, and D.G. Nathan, eds. (Philadelphia: Saunders), pp. 743–781.

Beroukhim, R., Mermel, C.H., Porter, D., Wei, G., Raychaudhuri, S., Donovan, J., Barretina, J., Boehm, J.S., Dobson, J., Urashima, M., et al. (2010). The

landscape of somatic copy-number alteration across human cancers. Nature *463*, 899–905.

Bignell, G.R., Greenman, C.D., Davies, H., Butler, A.P., Edkins, S., Andrews, J.M., Buck, G., Chen, L., Beare, D., Latimer, C., et al. (2010). Signatures of mutation and selection in the cancer genome. Nature *463*, 893–898.

Brüning, J.C., Michael, M.D., Winnay, J.N., Hayashi, T., Hörsch, D., Accili, D., Goodyear, L.J., and Kahn, C.R. (1998). A muscle-specific insulin receptor knockout exhibits features of the metabolic syndrome of NIDDM without altering glucose tolerance. Mol. Cell *2*, 559–569.

Chen, Y., Takita, J., Mizuguchi, M., Tanaka, K., Ida, K., Koh, K., Igarashi, T., Hanada, R., Tanaka, Y., Park, M.J., and Hayashi, Y. (2007). Mutation and expression analyses of the MET and CDKN2A genes in rhabdomyosarcoma with emphasis on MET overexpression. Genes Chromosomes Cancer *46*, 348–358.

Corcoran, R.B., and Scott, M.P. (2001). A mouse model for medulloblastoma and basal cell nevus syndrome. J. Neurooncol. *53*, 307–318.

Cypess, A.M., Lehman, S., Williams, G., Tal, I., Rodman, D., Goldfine, A.B., Kuo, F.C., Palmer, E.L., Tseng, Y.H., Doria, A., et al. (2009). Identification and importance of brown adipose tissue in adult humans. N. Engl. J. Med. *360*, 1509–1517.

El-Badry, O.M., Minniti, C., Kohn, E.C., Houghton, P.J., Daughaday, W.H., and Helman, L.J. (1990). Insulin-like growth factor II acts as an autocrine growth and motility factor in human rhabdomyosarcoma tumors. Cell Growth Differ. *1*, 325–331.

Engleka, K.A., Gitler, A.D., Zhang, M., Zhou, D.D., High, F.A., and Epstein, J.A. (2005). Insertion of Cre into the Pax3 locus creates a new allele of Splotch and identifies unexpected Pax3 derivatives. Dev. Biol. *280*, 396–406.

Estep, A.L., Tidyman, W.E., Teitell, M.A., Cotter, P.D., and Rauen, K.A. (2006). HRAS mutations in Costello syndrome: detection of constitutional activating mutations in codon 12 and 13 and loss of wild-type allele in malignancy. Am. J. Med. Genet. A. *140*, 8–16.

Fan, C.M., and Tessier-Lavigne, M. (1994). Patterning of mammalian somites by surface ectoderm and notochord: evidence for sclerotome induction by a hedgehog homolog. Cell *79*, 1175–1186.

Fukada, S., Uezumi, A., Ikemoto, M., Masuda, S., Segawa, M., Tanimura, N., Yamamoto, H., Miyagoe-Suzuki, Y., and Takeda, S. (2007). Molecular signature of quiescent satellite cells in adult skeletal muscle. Stem Cells *25*, 2448–2459.

Galindo, R.L., Allport, J.A., and Olson, E.N. (2006). A Drosophila model of the rhabdomyosarcoma initiator PAX7-FKHR. Proc. Natl. Acad. Sci. USA *103*, 13439–13444.

Gattenloehner, S., Vincent, A., Leuschner, I., Tzartos, S., Müller-Hermelink, H.K., Kirchner, T., and Marx, A. (1998). The fetal form of the acetylcholine receptor distinguishes rhabdomyosarcomas from other childhood tumors. Am. J. Pathol. *152*, 437–444.

Glüer, S., Schelp, C., von Schweinitz, D., and Gerardy-Schahn, R. (1998). Polysialylated neural cell adhesion molecule in childhood rhabdomyosarcoma. Pediatr. Res. *43*, 145–147.

Hahn, H., Wojnowski, L., Specht, K., Kappler, R., Calzada-Wack, J., Potter, D., Zimmer, A., Müller, U., Samson, E., Quintanilla-Martinez, L., and Zimmer, A. (2000). Patched target Igf2 is indispensable for the formation of medulloblastoma and rhabdomyosarcoma. J. Biol. Chem. *275*, 28341–28344.

He, W., Barak, Y., Hevener, A., Olson, P., Liao, D., Le, J., Nelson, M., Ong, E., Olefsky, J.M., and Evans, R.M. (2003). Adipose-specific peroxisome proliferator-activated receptor gamma knockout causes insulin resistance in fat and liver but not in muscle. Proc. Natl. Acad. Sci. USA *100*, 15712–15717.

Hettmer, S., and Wagers, A.J. (2010). Muscling in: uncovering the origins of rhabdomyosarcoma. Nat. Med. *16*, 171–173.

Hettmer, S., Liu, J., Miller, C.M., Lindsay, M.C., Sparks, C.A., Guertin, D.A., Bronson, R.T., Langenau, D.M., and Wagers, A.J. (2011). Sarcomas induced in discrete subsets of prospectively isolated skeletal muscle cells. Proc. Natl. Acad. Sci. USA *108*, 20002–20007.

Heyn, R., Newton, W.A., Raney, R.B., Hamoudi, A., Bagwell, C., Vietti, T., Wharam, M., Gehan, E., and Maurer, H.M. (1997). Preservation of the bladder in patients with rhabdomyosarcoma. J. Clin. Oncol. *15*, 69–75.

Iolascon, A., Faienza, M.F., Coppola, B., Rosolen, A., Basso, G., Della Ragione, F., and Schettini, F. (1996). Analysis of cyclin-dependent kinase inhibitor genes (CDKN2A, CDKN2B, and CDKN2C) in childhood rhabdomyosarcoma. Genes Chromosomes Cancer *15*, 217–222.

Ishiguro, N., Motoi, T., Araki, N., Ito, H., Moriyama, M., and Yoshida, H. (2008). Expression of cardiac ankyrin repeat protein, CARP, in malignant tumors: diagnostic use of CARP protein immunostaining in rhabdomyosarcoma. Hum. Pathol. *39*, 1673–1679.

Johnson, R.A., Wright, K.D., Poppleton, H., Mohankumar, K.M., Finkelstein, D., Pounds, S.B., Rand, V., Leary, S.E., White, E., Eden, C., et al. (2010). Cross-species genomics matches driver mutations and cell compartments to model ependymoma. Nature *466*, 632–636.

Johnson, R.L., Laufer, E., Riddle, R.D., and Tabin, C. (1994). Ectopic expression of Sonic hedgehog alters dorsal-ventral patterning of somites. Cell *79*, 1165–1173.

Johnson, R.L., Rothman, A.L., Xie, J., Goodrich, L.V., Bare, J.W., Bonifas, J.M., Quinn, A.G., Myers, R.M., Cox, D.R., Epstein, E.H., Jr., and Scott, M.P. (1996). Human homolog of patched, a candidate gene for the basal cell nevus syndrome. Science *272*, 1668–1671.

Kajimura, S., Seale, P., Kubota, K., Lunsford, E., Frangioni, J.V., Gygi, S.P., and Spiegelman, B.M. (2009). Initiation of myoblast to brown fat switch by a PRDM16-C/EBP-beta transcriptional complex. Nature *460*, 1154–1158.

Keller, C., and Capecchi, M.R. (2005). New genetic tactics to model alveolar rhabdomyosarcoma in the mouse. Cancer Res. *65*, 7530–7532.

Lee, Y., Kawagoe, R., Sasai, K., Li, Y., Russell, H.R., Curran, T., and McKinnon, P.J. (2007). Loss of suppressor-of-fused function promotes tumorigenesis. Oncogene *26*, 6442–6447.

Lepper, C., Conway, S.J., and Fan, C.M. (2009). Adult satellite cells and embryonic muscle progenitors have distinct genetic requirements. Nature *460*, 627–631.

Li, F.P., and Fraumeni, J.F., Jr. (1969). Rhabdomyosarcoma in children: epidemiologic study and identification of a familial cancer syndrome. J. Natl. Cancer Inst. *43*, 1365–1373.

Li, S., Czubryt, M.P., McAnally, J., Bassel-Duby, R., Richardson, J.A., Wiebel, F.F., Nordheim, A., and Olson, E.N. (2005). Requirement for serum response factor for skeletal muscle growth and maturation revealed by tissue-specific gene deletion in mice. Proc. Natl. Acad. Sci. USA *102*, 1082–1087.

Lum, L., and Beachy, P.A. (2004). The hedgehog response network: sensors, switches, and routers. Science *304*, 1755–1759.

Mao, J., Ligon, K.L., Rakhlin, E.Y., Thayer, S.P., Bronson, R.T., Rowitch, D., and McMahon, A.P. (2006). A novel somatic mouse model to survey tumorigenic potential applied to the hedgehog pathway. Cancer Res. *66*, 10171–10178.

Münsterberg, A.E., Kitajewski, J., Bumcrot, D.A., McMahon, A.P., and Lassar, A.B. (1995). Combinatorial signaling by Sonic hedgehog and Wnt family members induces myogenic bHLH gene expression in the somite. Genes Dev. *9*, 2911–2922.

Paulson, V., Chandler, G., Rakheja, D., Galindo, R.L., Wilson, K., Amatruda, J.F., and Cameron, S. (2011). High-resolution array CGH identifies common mechanisms that drive embryonal rhabdomyosarcoma pathogenesis. Genes Chromosomes Cancer *50*, 397–408.

Pressey, J.G., Anderson, J.R., Crossman, D.K., Lynch, J.C., and Barr, F.G. (2011). Hedgehog pathway activity in pediatric embryonal rhabdomyosarcoma and undifferentiated sarcoma: a report from the Children's Oncology Group. Pediatr. Blood Cancer *57*, 930–938.

Rezvani, G., Lui, J.C., Barnes, K.M., and Baron, J. (2012). A set of imprinted genes required for normal body growth also promotes growth of rhabdomyosarcoma cells. Pediatr. Res. *71*, 32–38.

Ross, S.R., Graves, R.A., Greenstein, A., Platt, K.A., Shyu, H.L., Mellovitz, B., and Spiegelman, B.M. (1990). A fat-specific enhancer is the primary

determinant of gene expression for adipocyte P2 in vivo. Proc. Natl. Acad. Sci. USA *87*, 9590–9594.

Ross, S.R., Choy, L., Graves, R.A., Fox, N., Solevjeva, V., Klaus, S., Ricquier, D., and Spiegelman, B.M. (1992). Hibernoma formation in transgenic mice and isolation of a brown adipocyte cell line expressing the uncoupling protein gene. Proc. Natl. Acad. Sci. USA *89*, 7561–7565.

Rubin, B.P., Nishijo, K., Chen, H.I., Yi, X., Schuetze, D.P., Pal, R., Prajapati, S.I., Abraham, J., Arenkiel, B.R., Chen, Q.R., et al. (2011). Evidence for an unanticipated relationship between undifferentiated pleomorphic sarcoma and embryonal rhabdomyosarcoma. Cancer Cell *19*, 177–191.

Seale, P., and Rudnicki, M.A. (2000). A new look at the origin, function, and "stem-cell" status of muscle satellite cells. Dev. Biol. *218*, 115–124.

Seale, P., Bjork, B., Yang, W., Kajimura, S., Chin, S., Kuang, S., Scimè, A., Devarakonda, S., Conroe, H.M., Erdjument-Bromage, H., et al. (2008). PRDM16 controls a brown fat/skeletal muscle switch. Nature *454*, 961–967.

Shadrach, J.L., and Wagers, A.J. (2011). Stem cells for skeletal muscle repair. Philos. Trans. R. Soc. Lond. B Biol. Sci. *366*, 2297–2306.

Sharp, R., Recio, J.A., Jhappan, C., Otsuka, T., Liu, S., Yu, Y., Liu, W., Anver, M., Navid, F., Helman, L.J., et al. (2002). Synergism between INK4a/ARF inactivation and aberrant HGF/SF signaling in rhabdomyosarcomagenesis. Nat. Med. *8*, 1276–1280.

Soriano, P. (1999). Generalized lacZ expression with the ROSA26 Cre reporter strain. Nat. Genet. *21*, 70–71.

Spunt, S.L., Lobe, T.E., Pappo, A.S., Parham, D.M., Wharam, M.D., Jr., Arndt, C., Anderson, J.R., Crist, W.M., Paidas, C., Wiener, E., et al. (2000). Aggressive surgery is unwarranted for biliary tract rhabdomyosarcoma. J. Pediatr. Surg. *35*, 309–316.

Srinivas, S., Watanabe, T., Lin, C.S., William, C.M., Tanabe, Y., Jessell, T.M., and Costantini, F. (2001). Cre reporter strains produced by targeted insertion of EYFP and ECFP into the ROSA26 locus. BMC Dev. Biol. *1*, 4.

Suh, J.M., Gao, X., McKay, J., McKay, R., Salo, Z., and Graff, J.M. (2006). Hedgehog signaling plays a conserved role in inhibiting fat formation. Cell Metab. *3*, 25–34.

Tallquist, M.D., Weismann, K.E., Hellström, M., and Soriano, P. (2000). Early myotome specification regulates PDGFA expression and axial skeleton development. Development *127*, 5059–5070.

Tang, W., Zeve, D., Suh, J.M., Bosnakovski, D., Kyba, M., Hammer, R.E., Tallquist, M.D., and Graff, J.M. (2008). White fat progenitor cells reside in the adipose vasculature. Science *322*, 583–586.

Tiffin, N., Williams, R.D., Shipley, J., and Pritchard-Jones, K. (2003). PAX7 expression in embryonal rhabdomyosarcoma suggests an origin in muscle satellite cells. Br. J. Cancer *89*, 327–332.

Tostar, U., Malm, C.J., Meis-Kindblom, J.M., Kindblom, L.G., Toftgård, R., and Undén, A.B. (2006). Deregulation of the hedgehog signalling pathway: a possible role for the PTCH and SUFU genes in human rhabdomyoma and rhabdomyosarcoma development. J. Pathol. *208*, 17–25.

Urs, S., Harrington, A., Liaw, L., and Small, D. (2006). Selective expression of an aP2/Fatty Acid Binding Protein 4-Cre transgene in non-adipogenic tissues during embryonic development. Transgenic Res. *15*, 647–653.

van Marken Lichtenbelt, W.D., Vanhommerig, J.W., Smulders, N.M., Drossaerts, J.M., Kemerink, G.J., Bouvy, N.D., Schrauwen, P., and Teule, G.J. (2009). Cold-activated brown adipose tissue in healthy men. N. Engl. J. Med. *360*, 1500–1508.

Virtanen, K.A., Lidell, M.E., Orava, J., Heglind, M., Westergren, R., Niemi, T., Taittonen, M., Laine, J., Savisto, N.J., Enerbäck, S., and Nuutila, P. (2009). Functional brown adipose tissue in healthy adults. N. Engl. J. Med. *360*, 1518–1525.

Wang, Q., Fang, W.H., Krupinski, J., Kumar, S., Slevin, M., and Kumar, P. (2008). Pax genes in embryogenesis and oncogenesis. J. Cell. Mol. Med. *12* (6A), 2281–2294.

Williamson, D., Missiaglia, E., de Reyniès, A., Pierron, G., Thuille, B., Palenzuela, G., Thway, K., Orbach, D., Laé, M., Fréneaux, P., et al. (2010). Fusion gene-negative alveolar rhabdomyosarcoma is clinically and molecularly indistinguishable from embryonal rhabdomyosarcoma. J. Clin. Oncol. *28*, 2151–2158.

Yamamoto, M., Shook, N.A., Kanisicak, O., Yamamoto, S., Wosczyna, M.N., Camp, J.R., and Goldhamer, D.J. (2009). A multifunctional reporter mouse line for Cre- and FLP-dependent lineage analysis. Genesis *47*, 107–114.

Zibat, A., Missiaglia, E., Rosenberger, A., Pritchard-Jones, K., Shipley, J., Hahn, H., and Fulda, S. (2010). Activation of the hedgehog pathway confers a poor prognosis in embryonal and fusion gene-negative alveolar rhabdomyosarcoma. Oncogene *29*, 6323–6330.